Steering Large Magnetic Exchange Coupling in Nanographenes near the Closed-Shell to Open-Shell Transition

Kalyan Biswas,[†,♠] Diego Soler,[Δ,♠] Shantanu Mishra,[η,θ,♠] Qiang Chen,[‡,♠] Xuelin Yao,[‡,♠] Ana Sánchez-Grande,[†] Kristjan Eimre,[η] Pingo Mutombo,[Δ] Cristina Martín-Fuentes,[†] Koen Lauwaet,[†] José M. Gallego,[ρ] Pascal Ruffieux,[η] Carlo A. Pignedoli,[η] Klaus Müllen,[‡] Rodolfo Miranda,[†,φ] José I. Urgel,[†,*] Akimitsu Narita,[‡,*] Roman Fasel,[η,ς,*] Pavel Jelínek,[Δ,ψ,*] and David Écija[†,*]

[†] IMDEA Nanoscience, C/ Faraday 9, Campus de Cantoblanco, 28049 Madrid, Spain

[Δ] Institute of Physics of the Czech Academy of Science, Praha 162 00, Czech Republic

[η] Empa, Swiss Federal Laboratories for Materials Science and Technology, 8600 Dübendorf, Switzerland

[θ] IBM Research – Zurich, Säumerstrasse 4, 8803 Rüschlikon, Switzerland

[‡] Max Planck Institute for Polymer Research, 55128 Mainz, Germany

[ρ] Instituto de Ciencia de Materiales de Madrid, CSIC, Cantoblanco, 28049 Madrid, Spain

[φ] Departamento de Física de la Materia Condensada, Universidad Autónoma de Madrid, 28049 Madrid, Spain

[ψ] Regional Centre of Advanced Technologies and Materials, Palacký University Olomouc, CZ-771 46 Olomouc, Czech Republic

[ς] Department of Chemistry, Biochemistry and Pharmaceutical Sciences, University of Bern, 3012 Bern, Switzerland

ABSTRACT: The design of open-shell carbon-based nanomaterials is at the vanguard of materials science, steered by their beneficial magnetic properties like weaker spin-orbit coupling than transition metal atoms and larger spin delocalization, which are of potential relevance for future spintronics and quantum technologies. A key parameter in magnetic materials is the magnetic exchange coupling between unpaired spins, which should be large enough to allow device operation at practical temperatures. In this work, we theoretically and experimentally explore three distinct families of nanographenes (**A**, **B** and **C**) featuring majority zigzag peripheries. Through many-body calculations, we identify a transition from a closed-shell to an open-shell ground state upon increase of the molecular size. Our predictions indicate that the largest magnetic exchange coupling for open-shell nanographenes occurs in proximity to the transition between closed-shell and open-shell states. Such predictions are corroborated by the on-surface syntheses, and structural, electronic and magnetic characterization of three nanographenes (**A[3,5]**, **B[4,5]** and **C[4,3]**), which are the smallest open-shell systems in their respective chemical families, and are thus located the closest to the transition boundary. Notably, two of the nanographenes (**B[4,5]** and **C[4,3]**) feature record values of magnetic exchange coupling (close to 200 meV) measured on the Au(111) surface. Our strategy for maximizing the magnetic exchange coupling provides perspectives for designing carbon nanomaterials with robust magnetic ground states.

INTRODUCTION

Carbon nanostructures may exhibit magnetism arising from π-electrons that is distinct from magnetism in materials containing transition metal ions.[1] Unpaired electrons in magnetic (open-shell) carbon-based nanomaterials are hosted by molecular orbitals, which leads to highly delocalized spin densities. This allows efficient control of the magnetic exchange coupling (MEC) through rational design of molecular size and shape.[2-4] In addition, carbon-based nanostructures are predicted to exhibit intrinsically weak spin-orbit and hyperfine couplings, which are major channels of spin relaxation and decoherence, and large spin stiffness values that may lead to augmented Curie temperatures.[5-8] Such outstanding properties make open-shell carbon-based nanomaterials promising for emerging technologies like spintronics and quantum computation.[9] Consequently, enormous efforts have been devoted to the synthesis of open-shell carbon nanostructures, with graphene nanoribbons (GNRs) and nanographenes (NGs) being outstanding examples.[2, 10] Synthesis of open-shell carbon-based nanomaterials in solution is frequently hampered by their high reactivity that arises from unpaired electrons. In this regard, on-surface synthesis under ultra-high vacuum (UHV) provides an attractive alternative to synthesize and stabilize reactive species on solid surfaces, while enabling their atomic-scale structural and electronic characterization using scanning probe microscopies.[3-4, 11-36]

A straightforward route to generate magnetism in carbon nanostructures is to induce a sublattice imbalance in the bipartite honeycomb lattice. This strategy gives rise to non-Kekulé molecules, where it is impossible to draw Kekulé resonance structures without leaving unpaired electrons.[3-4] An intuitive approach to attain sublattice imbalance is by creating defects in the honeycomb lattice that locally remove p_z orbitals. This can be achieved by (1) chemisorption of atoms,[37-38] (2) generation of carbon vacancies,[39] (3) introduction of odd-membered polycycles[18-19], and (4) heteroatom substitutions.[24,29] Alternatively, sublattice imbalance can also be expressed by designing NGs of specific shapes and edge structures, with a notable example being the family of triangulenes.[13, 16, 32] Non-Kekulé molecules may also be obtained without sublattice imbalance, but examples of such nanostructures remain rare.[17]

A distinct approach to express magnetism in NGs is to take advantage of the role of electronic correlations above a critical system size, which makes feasible that Coulomb repulsion overcomes the hybridization energy of the frontier states, giving rise to a net spin polarization.[4, 20, 30,31] Herein, the edge shape of the NG is very relevant, being the zigzag peripheries successful for achieving spin polarizations. A recent study exemplifying this concept reports on the on-surface synthesis of rhombus-shaped NGs with zigzag peripheries, containing four and five benzenoid rings along each edge (termed [4]- and [5]-rhombenes, respectively).[30] While [4]-rhombene was found to be non-magnetic (closed-shell), [5]-rhombene exhibited an open-shell singlet ground state with a large MEC of 102 meV.

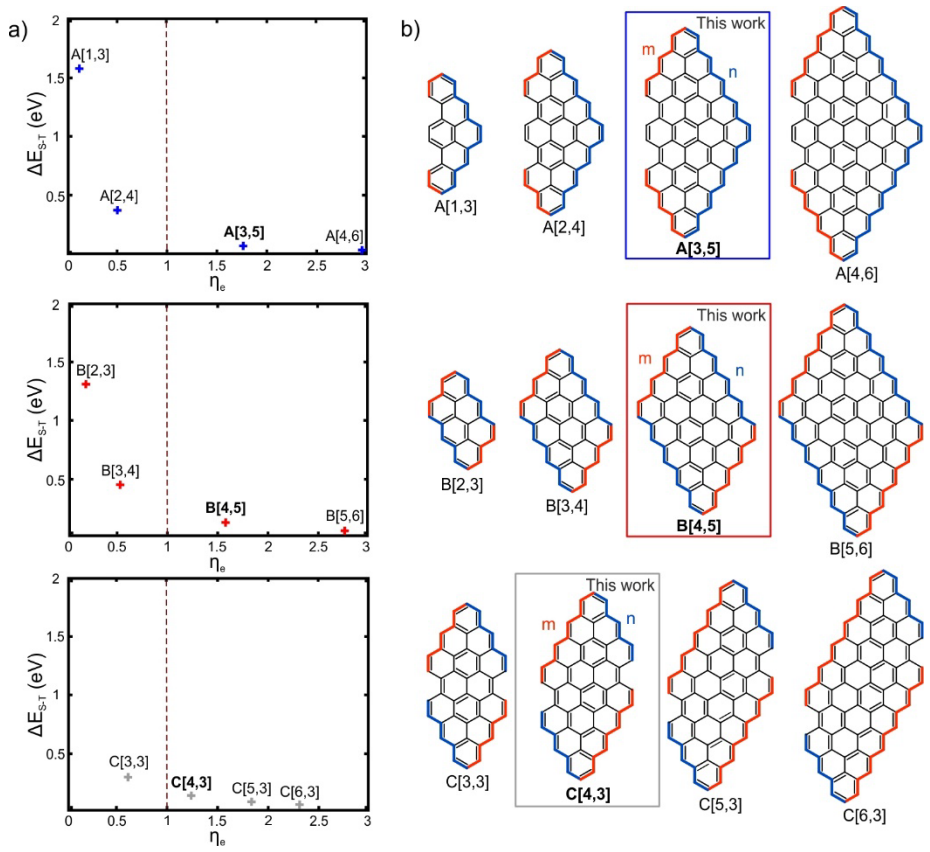

Figure 1. Theoretical survey of the open-shell character of the NGs in families A, B and C. (a) Graphs depicting the singlet-triplet excitation energies ($\Delta E_{S\text{-}T}$) *vs.* the number of unpaired electrons (η_e) for the first four members of **A**, **B** and **C**, obtained with an exact diagonalization of the Hubbard model. The dashed lines divide the boundary between closed-shell (left) and open-shell (right) regions (see text for details). (b) Chemical sketch of the first four members of **A**, **B** and **C**. The molecules highlighted with squares are studied in this work.

A large MEC is often desirable in the context of robustness of the magnetic ground state. MEC values larger than the Landauer limit of theoretical minimum energy dissipation[40] ($k_B T\ln(2) \approx 18$ meV at $T = 300$ K) are important to achieve both fast switching and fault-tolerant operation at reasonable temperatures.

However, there is currently a limited understanding of the tunability of MEC in open-shell carbon nanostructures. In our work, we address such challenge through a combined theoretical and experimental study of three families of NGs, viz. **A**, **B** and **C** (Fig. 1), which contain a majority of zigzag edges. Our many-body calculations reveal a size-dependent closed-shell to open-shell transition in NGs of the three families with increasing size. Furthermore, we find that within each family, the largest MEC for an open-shell NG is achieved when the NG lies near the boundary of the closed-shell to open-shell transition. Following our theoretical predictions, we perform the on-surface synthesis of the three open-shell NGs that are predicted to display the highest MEC, viz. **A[3,5]**, **B[4,5]** and **C[4,3]** (Fig.1, where the indices [m,n] denote the number of benzene rings along two adjacent zigzag edges of the NG). The corresponding precursor molecules **pA[3,5]**, **pB[4,5]** and **pC[4,3]** were synthesized in solution and sublimed on a Au(111) surface under UHV conditions, giving rise to **A[3,5]**, **B[4,5]** and **C[4,3]**, respectively, upon thermal annealing. The elucidation of their resulting structure and electronic properties is addressed by using scanning tunneling microscopy (STM) and scanning tunneling spectroscopy (STS) at 4.3 K. Notably, our measurements reveal that NGs **A[3,5]**, **B[4,5]** and **C[4,3]** exhibit MEC values of 116, 183 and 190 meV, respectively, thus achieving the largest MEC reported to date for on-surface synthesized carbon nanostructures.

RESULTS AND DISCUSSION.

We first theoretically studied the closed-shell to open-shell transition upon increase of the molecular size of the above-mentioned families of NGs. To this end, we obtained the many-body ground state and the magnetic excitation spectra of the selected NGs by solving the Hubbard model using exact diagonalization (ED) in a reduced active space (see Supplementary Information for details). We determined the open-shell character according to the occupation number of the natural orbitals,[41] which yields the number of unpaired electrons η_e.[42] As an orientative threshold, a value of η_e larger than 1 is taken to mark the (gradual) transition from closed-shell to open-shell (see discussion in Supplementary Information).

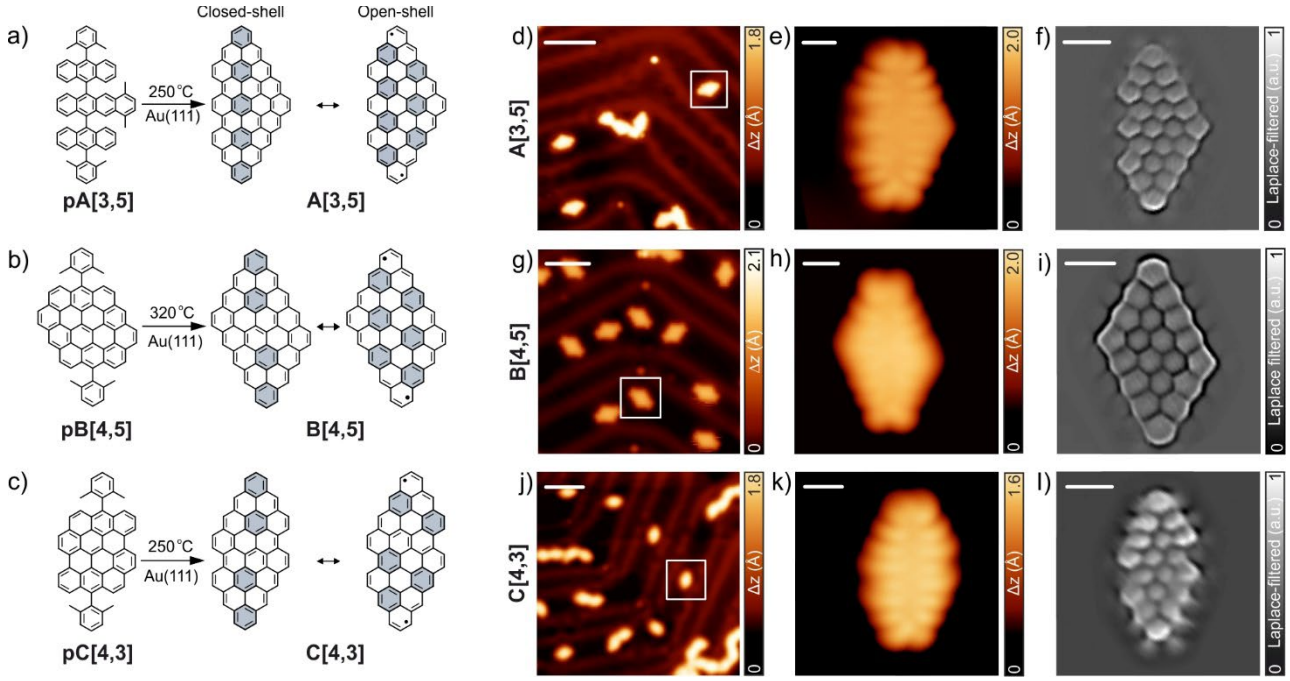

Figure 2. On-surface syntheses and structural characterization of A[3,5], B[4,5] and C[4,3]. (a-c) Schematic representation of on-surface syntheses of (a) **A[3,5]**, (b) **B[4,5]** and (c) **C[4,3]** on Au(111). Grey filled rings highlight Clar's sextets. **(d, g, j)** Overview STM images after annealing (d) **pA[3,5]** at 250 °C, (g) **pB[4,5]** at 320 °C and (j) **pC[4,3]** at 250 °C on Au(111). White squares in the respective images highlight isolated **A[3,5], B[4,5] and C[4,3]** molecules. **(e, h, k)** High-resolution STM images of (e) **A[3,5]**, (h) **B[4,5]** and (k) **C[4,3]**. **(f, i, l)** Laplace-filtered ultra-high resolution STM images of (f) **A[3,5]**, (i) **B[4,5]** and (l) **C[4,3]**. Images in panels (e), (f), (h), (i), (k) and (l) are acquired with a CO-functionalized tip. Tunneling parameters for STM images: (d) $V = 200$ mV, $I = 10$ pA; (e) $V = -300$ mV, $I = 300$ pA; (f) $V = 5$ mV, $I = 50$ pA, $Z_{offset} = 120$ pm; (g) $V = -700$ mV, $I = 40$ pA; (h) $V = -300$ mV, $I = 280$ pA; (i) $V = -5$ mV, $I = 50$ pA, $Z_{offset} = -95$ pm; (j) $V = 200$ mV, $I = 120$ pA; (k) $V = -300$ mV, $I = 300$ pA; (l) $V = 5$ mV, $I = 50$ pA, $Z_{offset} = 100$ pm. Scale bars: (d) 5 nm, (g) 4 nm, (j) 5 nm, (e-f) 0.5 nm, (h-i) 0.5 nm, (k-l) 0.5 nm. Z_{offset} denotes the offset applied to the tip–sample distance with respect to the STM setpoint above the NGs. Positive and negative values of Z_{offset} denote tip approach and retraction from the setpoint, respectively.

Figure 1a shows plots of the singlet-triplet ($S = 0$ to $S = 1$) spin excitation energies versus the number of unpaired electrons for the first four members of each of the three families of NGs (Fig. 1b). We note that the magnetic ground state for all open-shell NGs is a singlet (in accordance with Lieb's theorem), while the first excited state for all NGs, irrespective of their open-shell or closed-shell ground state, is a triplet. The singlet-triplet spin excitation energies, which provide a direct measure of the MEC, are obtained as the difference of the first two eigenvalues of the many-body Hamiltonian matrix of the Hubbard model, which is diagonalized exactly in the reduced active space of six molecular orbitals (see Supplementary Information for details). As seen in Fig. 1a, the largest MEC for the open-shell NGs of a given family is always observed for those that are located nearest to the closed-shell to open-shell transition, which are NGs **A[3,5]**, **B[4,5]** and **C[4,3]** (see Table I in Supplementary Information for calculated values).

Motivated by our theoretical predictions, we next focused our attention on the syntheses of NGs **A[3,5]**, **B[4,5]** and **C[4,3]** on a Au(111) surface and their in-depth structural and electronic characterization, targeting to achieve the design of the nanographenes exhibiting the highest reported MEC on surfaces.

To this aim, during our synthetic exploration of various NGs with a combination of zigzag and armchair edges, we conceived the molecular precursors **pA[3,5]**, **pB[4,5]**, and **pC[4,3]**, which were expected to yield **A[3,5]**, **B[4,5]** and **C[4,3]** on Au(111), respectively, through surface-catalyzed oxidative cyclization and dehydrogenation reactions (Fig. 2a-c). The preparation of **pC[4,3]** was previously described,[43] and **pA[3,5]** and **pB[4,5]** were synthesized by adapting our reported procedures (cf. Supporting Information for details).[30, 44-45]

Figures 2d, g, j show overview STM images after deposition of the precursor molecules on Au(111) held at room temperature and subsequent annealing of the surface. The images reveal the presence of individual molecules highlighted by white squares, which are tentatively assigned to **A[3,5]**, **B[4,5]** and **C[4,3]**. In addition, overview images also display several byproducts, whose formation is due to concomitant non-selective dehydrogenative carbon-carbon (C-C) coupling reactions that occur at the annealing temperature. A statistical analysis of over 100 imaged species revealed that ~ 10%, 63% and 14% of the species on the surface correspond to **A[3,5]**, **B[4,5]** and **C[4,3]**, respectively.

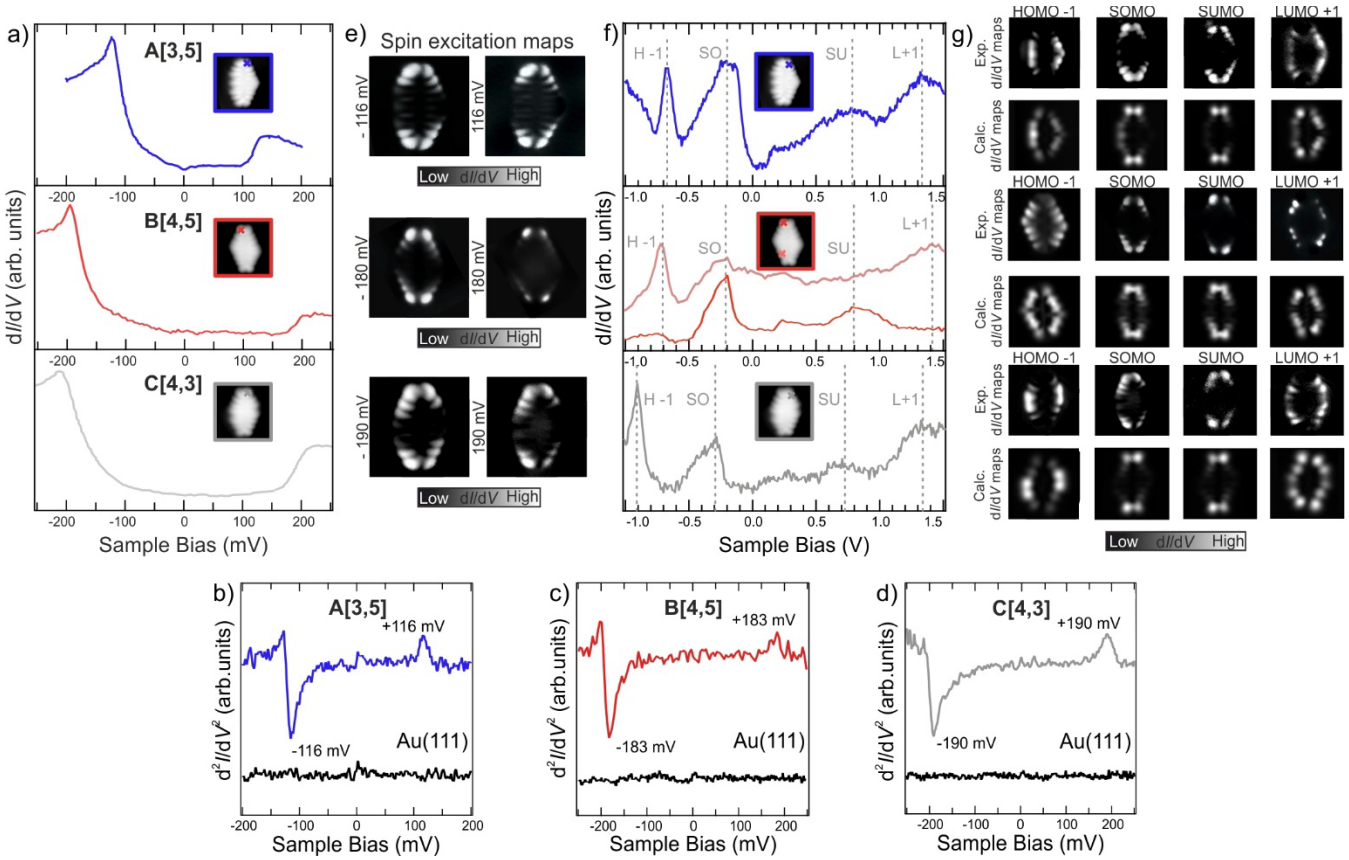

Figure 3. Electronic and magnetic characterization of A[3,5], B[4,5] and C[4,3]. (a) d*I*/d*V* spectra obtained on **A[3,5]**, **B[4,5]** and **C[4,3]**. Acquisition positions are indicated by colored crosses in the inset STM images. Open feedback parameters: $V = 0.20$ V, $I = 450$ pA, root mean squared modulation voltage $V_{rms} = 4$ mV for **A[3,5]**; $V = -0.30$ V, $I = 750$ pA, $V_{rms} = 1$ mV for **B[4,5]**; and $V = 0.25$ V, $I = 300$ pA, $V_{rms} = 10$ mV for **C[4,3]**. (b-d) d^2I/dV^2 spectra on **A[3,5]**, **B[4,5]** and **C[4,3]** at the positions indicated in the inset STM images in (a). Open feedback parameters for d^2I/dV^2 spectroscopy: (b) $V = 0.25$ V, $I = 450$ pA, $V_{rms} = 4$ mV; (c) $V = -0.25$ V, $I = 750$ pA, $V_{rms} = 1$ mV; (d) $V = 0.25$ V, $I = 450$ pA, $V_{rms} = 6$ mV. (e) Constant-current d*I*/d*V* maps of the NGs near their respective spin excitation energies ($I = 350$ pA and $V_{rms} = 10$ mV). (f) Long-range d*I*/d*V* spectra acquired on **A[3,5]**, **B[4,5]** and **C[4,3]** ($I = 100$ pA and $V_{rms} = 20$ mV). Acquisition positions are indicated by colored crosses in the inset STM images. The labels H–1, SO, SU and L+1 indicate the HOMO−1, SOMO, SUMO (SUMO denotes the corresponding unoccupied counterpart of SOMO) and LUMO+1 resonance peaks, respectively. (g) Experimental constant-current d*I*/d*V* maps and DFT-calculated d*I*/d*V* maps acquired at the molecular orbital resonances for each NG. Tunneling parameters for the experimental d*I*/d*V* maps: H–1 ($V = -0.60$ V, $I = 200$ pA), SO ($V = -0.20$ V, $I = 300$ pA), SU ($V = 0.75$ V, $I = 300$ pA) and L + 1 ($V = 1.4$ V, $I = 400$ pA) with $V_{rms} = 20$ mV for **A[3,5]**; H – 1 ($V = -0.70$ V, $I = 280$ pA), SO ($V = -0.30$ V, $I = 280$ pA), SU ($V = 0.60$ V, $I = 320$ pA) and L + 1 ($V = 1.40$ V, $I = 320$ pA) with $V_{rms} = 24$ mV for **B[4,5]**; H – 1 ($V = -0.88$ V, $I = 300$ pA), SO ($V = -0.30$ V, $I = 300$ pA), SU ($V = 0.70$ V, $I = 300$ pA) and L + 1 ($V = 1.50$ V, $I = 300$ pA) with $V_{rms} = 20$ mV for **C[4,3]**.

Figures 2e,h,k display high-resolution STM images of **A[3,5]**, **B[4,5]** and **C[4,3]**, respectively, where a characteristic modulation in the local density of states is observed along the periphery of the NGs, which, as it is shown later, results from localized states at the extended zigzag edges of the NGs.[46-47] Finally, we performed ultra-high resolution STM imaging with a CO functionalized tip, which confirmed the chemical structures of the three NGs, and revealed their stable and planar adsorption geometries on Au(111) (Figures 2f,i,l).

The electronic structure of **A[3,5]**, **B[4,5]** and **C[4,3]** was probed by STS, combining differential conductance spectroscopy (*dI*/*dV* *vs.* *V*, where *I* and *V* denote the tunneling current and bias voltage) with spatially-resolved d*I*/d*V* mapping. Figure 3a shows high-resolution d*I*/d*V* spectra on **A[3,5]**, **B[4,5]** and **C[4,3]**, where we observe peaked steps in conductance symmetric around the Fermi energy (see discussion about the shape of the graphs in Supplementary Information).[12] The energetic positions of the steps are found to be at ±116, ±183 and ±190 meV for **A[3,5]**, **B[4,5]** and **C[4,3]**, respectively, using d^2I/dV^2 spectroscopy (Fig. 3b–d). Stepwise changes in d*I*/d*V* are indicative of inelastic excitations. Based on our theoretical predictions, along with the reasonable agreement with the DFT-predicted singlet-triplet gaps of **A[3,5]** (114 meV), **B[4,5]** (192 meV) and **C[4,3]** (225 meV) (see Table II in Supplementary Information), we ascribe the d*I*/d*V* steps to singlet-triplet spin excitations in the NGs.[12, 17, 20, 30-31] We also obtained d*I*/d*V* maps at the spin excitation thresholds (Fig. 3e), which are in line with the calculated spin polarization plots of the respective NGs (see Supplementary Information).

Additionally, we performed d*I*/d*V* spectroscopy on **A[3,5]**, **B[4,5]** and **C[4,3]** in a larger bias windows to detect orbital resonances. All the three NGs exhibit four electronic resonances at −0.60 V, −0.20 V, 0.75 V and 1.40 V (**A[3,5]**); −0.70 V, −0.30 V, 0.60 V and 1.40 V (**B[4,5]**) and −0.88 V, −0.30 V, 0.70 V and 1.50 V (**C[4,3]**) (Fig. 3f). Based on comparisons of the experimental d*I*/d*V* maps at these resonances with the DFT-calculated d*I*/d*V* maps of the NGs (Fig. 3g), we assign the pairs of resonances at −0.60 V/1.40 V (**A[3,5]**), −0.70 V/1.40 V (**B[4,5]**) and −0.88 V/1.50 V (**C[4,3]**) to tunneling through the HOMO–1/LUMO+1 of the NGs. In addition, d*I*/d*V* maps at the frontier resonances, *viz.* −0.20 V/0.75 V (**A[3,5]**), −0.30 V/0.60 V (**B[4,5]**) and −0.30 V/0.70 V (**C[4,3]**)

exhibit similar shapes and symmetries at both bias polarities, which indicates tunneling to/from the same orbitals. Based on this and from comparison of the experimental d*I*/d*V* maps with the DFT-calculated d*I*/d*V* maps (Fig. 3g), we ascribe the frontier resonances to tunneling to/from the SUMO/SOMO of the NGs, which further supports the open-shell ground states of **A[3,5]**, **B[4,5]** and **C[4,3]**. The frontier electronic gaps of **A[3,5]**, **B[4,5]** and **C[4,3]** are deduced to be 0.95, 0.90 and 1.00 eV, respectively. Finally, for both the closed- and open-shell states of the NGs, we performed many-body perturbation theory calculations in the GW approximation (where G and W denote Green's function and the screened Coulomb potential, respectively), together with image charge (IC) corrections, which include screening effects from the underlying Au(111) surface (see Table II in Supplementary Information). For all NGs, the experimental frontier gap shows a better agreement with the GW+IC gap for the open-shell singlet state than for the closed-shell state, providing further evidence for the open-shell nature of these structures.

Conclusion

MEC in open-shell carbon nanostructures is an important parameter that governs the robustness of the magnetic ground state against external fluctuations such as temperature. In addition, a large MEC is imperative for spin-logic operations at practical temperatures. Our work therefore strives to address the general issue of tunability of MEC in open-shell carbon nanostructures. To this end, we perform a detailed theoretical and experimental study on three chemical families of NGs, *viz.* **A**, **B** and **C**, which contain a majority of zigzag edges. Our ab-initio and many-body theoretical analyses reveal that for each of these families, there is a size-dependent closed-shell to open-shell transition beyond a critical system size. Furthermore, we show that for open-shell NGs of a given family, the largest MEC is achieved for the NG that lies closest to the closed-shell to open-shell transition boundary (which, for the three families, correspond to the NGs **A[3,5]**, **B[4,5]** and **C[4,3]**). To corroborate our theoretical findings, we perform the on-surface syntheses of the aforementioned NGs and explore their electronic structure using STM and STS at submolecular resolution. Consistent with the theoretical picture, we find that **A[3,5]**, **B[4,5]** and **C[4,3]** exhibit open-shell ground states. Markedly, for these three NGs, we find large values of MEC, *viz.* 116 (**A[3,5]**), 183 (**B[4,5]**) and 190 meV (**C[4,3]**), thus achieving the largest MEC value reported to date for carbon nanostructures on surfaces.

Our work highlights the importance of theoretical analysis for predicting large magnetic exchange coupling and the enormous capabilities of organic chemistry and on-surface synthesis for bringing such predictions into reality, giving rise to record values for singlet-triplet excitations in π-directed magnetism on surfaces.

ASSOCIATED CONTENT

Supporting Information. The Supporting Information is available free of charge on the ACS Publications website at DOI: Experimental details, synthesis, characterizations, computational studies, and NMR spectra (PDF)

AUTHOR INFORMATION

Corresponding Authors

José I. Urgel − Email: jose-ignacio.urgel@imdea.org

Akimitsu Narita − Email: akimitsu.narita@oist.jp

Roman Fasel − Email: roman.fasel@empa.ch

Pavel Jelínek − Email: jelinekp@fzu.cz

David Écija − Email: david.ecija@imdea.org

Authors

ORCID

Kalyan Biswas − orcid.org/0000-0002-1951-5595

Diego Soler − orcid.org/ 0000-0001-9215-4151

Shantanu Mishra − orcid.org/ 0000-0002-2900-4203

Qiang Chen − orcid.org/ 0000-0001-5612-1504

Ana Sánchez-Grande − orcid.org/ 0000-0002-5499-0199

Kristjan Eimre − orcid.org/ 0000-0002-3444-3286

Koen Lauwaet − orcid.org/ 0000-0003-1024-6779

José M. Gallego − orcid.org/ 0000-0003-1716-0126

Pascal Ruffieux − orcid.org/ 0000-0001-5729-5354

Carlo A. Pignedoli − orcid.org/ 0000-0002-8273-6390

Klaus Müllen − orcid.org/ 0000-0001-6630-8786

Rodolfo Miranda − orcid.org/ 0000-0002-1064-6724

José I. Urgel − orcid.org/ 0000-0001-7608-2979

Akimitsu Narita − orcid.org/ 0000-0002-3625-522X

Roman Fasel − orcid.org/ 0000-0002-1553-6487

Pavel Jelínek − orcid.org/ 0000-0002-5645-8542

David Écija − orcid.org/ 0000-0002-8661-8295

Notes

The authors declare no competing financial interest.

♠ Equally contributing author.

ACKNOWLEDGMENT

The authors acknowledge the Comunidad de Madrid [project QUIMTRONIC-CM (Y2018/NMT-4783)], Ministerio de Ciencia e Innovación (PID2019-108532GB-I00), the Max Planck Society, the ANR-DFG NLE Grant GRANAO by DFG 431450789, and the NCCR MARVEL funded by the Swiss National Science Foundation (grant no. 51NF40-205602). IMDEA Nanociencia thanks support from the "Severo Ochoa" Programme for Centers of Excellence in R&D (MINECO, Grant SEV-2016-0686 and CEX2020-001039-S). J.I.U. acknowledges the funding from the European Union's Horizon 2020 research and innovation programme under the Marie Skłodowska-Curie grant agreement no. 886314. K.M. appreciates a fellowship from Gutenberg Research College, Johannes Gutenberg University Mainz. The Swiss National Supercomputing Centre (CSCS) under project ID s1141 is acknowledged for computational resources.

REFERENCES

1. Yazyev, O. V., Emergence of magnetism in graphene materials and nanostructures. Rep. Prog. Phys. 2010, 73 (5), 056501.
2. Zeng, W.; Wu, J., Open-Shell Graphene Fragments. Chem 2021, 7 (2), 358-386.
3. Song, S.; Su, J.; Telychko, M.; Li, J.; Li, G.; Li, Y.; Su, C.; Wu, J.; Lu, J., On-surface synthesis of graphene nanostructures with π-magnetism. Chem. Soc. Rev. 2021, 50 (5), 3238-3262.
4. de Oteyza, D. G.; Frederiksen, T., Carbon-based nanostructures as a versatile platform for tunable π-magnetism. J. Phys. Cond. Matter 2022, 34, 443001.
5. Yazyev, O. V.; Katsnelson, M. I., Magnetic Correlations at Graphene Edges: Basis for Novel Spintronics Devices. Phys. Rev. Lett. 2008, 100 (4), 047209.

6. Trauzettel, B.; Bulaev, D. V.; Loss, D.; Burkard, G., Spin qubits in graphene quantum dots. Nat. Phys. 2007, 3 (3), 192-196.
7. Yazyev, O. V., Hyperfine Interactions in Graphene and Related Carbon Nanostructures. Nano Lett. 2008, 8 (4), 1011-1015.
8. Han, W.; Kawakami, R. K.; Gmitra, M.; Fabian, J., Graphene spintronics. Nat. Nanotechnol. 2014, 9 (10), 794-807.
9. Lombardi, F.; Lodi, A.; Ma, J.; Liu, J.; Slota, M.; Narita, A.; Myers, W. K.; Müllen, K.; Feng, X.; Bogani, L., Quantum units from the topological engineering of molecular graphenoids. Science 2019, 366 (6469), 1107-1110.
10. Wang, X.-Y.; Yao, X.; Müllen, K., Polycyclic aromatic hydrocarbons in the graphene era. Sci. China Chem. 2019, 62 (9), 1099-1144.
11. Clair, S.; de Oteyza, D. G., Controlling a Chemical Coupling Reaction on a Surface: Tools and Strategies for On-Surface Synthesis. Chem. Rev. 2019, 119 (7), 4717-4776.
12. Li, J.; Sanz, S.; Corso, M.; Choi, D. J.; Peña, D.; Frederiksen, T.; Pascual, J. I., Single spin localization and manipulation in graphene open-shell nanostructures. Nat. Commun. 2019, 10 (1), 200.
13. Mishra, S.; Beyer, D.; Eimre, K.; Liu, J.; Berger, R.; Gröning, O.; Pignedoli, C. A.; Müllen, K.; Fasel, R.; Feng, X.; Ruffieux, P., Synthesis and Characterization of π-Extended Triangulene. J. Am. Chem. Soc. 2019, 141 (27), 10621-10625.
14. Sánchez-Grande, A.; Urgel, J. I.; Cahlík, A.; Santos, J.; Edalatmanesh, S.; Rodríguez-Sánchez, E.; Lauwaet, K.; Mutombo, P.; Nachtigallová, D.; Nieman, R.; Lischka, H.; de la Torre, B.; Miranda, R.; Gröning, O.; Martín, N.; Jelínek, P.; Écija, D., Diradical Organic One-Dimensional Polymers Synthesized on a Metallic Surface. Angew. Chem. Int. Ed. 2020, 59 (40), 17594-17599.
15. Zheng, Y.; Li, C.; Xu, C.; Beyer, D.; Yue, X.; Zhao, Y.; Wang, G.; Guan, D.; Li, Y.; Zheng, H.; Liu, C.; Liu, J.; Wang, X.; Luo, W.; Feng, X.; Wang, S.; Jia, J., Designer spin order in diradical nanographenes. Nat. Commun. 2020, 11 (1), 6076.
16. Su, X.; Li, C.; Du, Q.; Tao, K.; Wang, S.; Yu, P., Atomically Precise Synthesis and Characterization of Heptauthrene with Triplet Ground State. Nano Lett. 2020, 20 (9), 6859-6864.
17. Mishra, S.; Beyer, D.; Eimre, K.; Kezilebieke, S.; Berger, R.; Gröning, O.; Pignedoli, C. A.; Müllen, K.; Liljeroth, P.; Ruffieux, P.; Feng, X.; Fasel, R., Topological frustration induces unconventional magnetism in a nanographene. Nat. Nanotechnol. 2020, 15 (1), 22-28.
18. Mishra, S.; Beyer, D.; Berger, R.; Liu, J.; Gröning, O.; Urgel, J. I.; Müllen, K.; Ruffieux, P.; Feng, X.; Fasel, R., Topological Defect-Induced Magnetism in a Nanographene. J. Am. Chem. Soc. 2020, 142 (3), 1147-1152.
19. Li, J.; Sanz, S.; Castro-Esteban, J.; Vilas-Varela, M.; Friedrich, N.; Frederiksen, T.; Peña, D.; Pascual, J. I., Uncovering the Triplet Ground State of Triangular Graphene Nanoflakes Engineered with Atomic Precision on a Metal Surface. Phys. Rev. Lett. 2020, 124 (17), 177201.
20. Sánchez-Grande, A.; Urgel, J. I.; Veis, L.; Edalatmanesh, S.; Santos, J.; Lauwaet, K.; Mutombo, P.; Gallego, J. M.; Brabec, J.; Beran, P.; Nachtigallová, D.; Miranda, R.; Martín, N.; Jelínek, P.; Écija, D., Unravelling the Open-Shell Character of Peripentacene on Au(111). J. Phys. Chem. Lett. 2021, 12 (1), 330-336.
21. Mishra, S.; Beyer, D.; Eimre, K.; Ortiz, R.; Fernández-Rossier, J.; Berger, R.; Gröning, O.; Pignedoli, C. A.; Fasel, R.; Feng, X.; Ruffieux, P., Collective All-Carbon Magnetism in Triangulene Dimers. Angew. Chem. Int. Ed. 2020, 59 (29), 12041-12047.
22. Hieulle, J.; Castro, S.; Friedrich, N.; Vegliante, A.; Lara, F. R.; Sanz, S.; Rey, D.; Corso, M.; Frederiksen, T.; Pascual, J. I.; Peña, D., On-Surface Synthesis and Collective Spin Excitations of a Triangulene-Based Nanostar. Angew. Chem. Int. Ed. 2021, 60 (48), 25224-25229.
23. Mishra, S.; Catarina, G.; Wu, F.; Ortiz, R.; Jacob, D.; Eimre, K.; Ma, J.; Pignedoli, C. A.; Feng, X.; Ruffieux, P.; Fernández-Rossier, J.; Fasel, R., Observation of fractional edge excitations in nanographene spin chains. Nature 2021, 598 (7880), 287-292.
24. Wang, T.; Sanz, S.; Castro-Esteban, J.; Lawrence, J.; Berdonces-Layunta, A.; Mohammed, M. S. G.; Vilas-Varela, M.; Corso, M.; Peña, D.; Frederiksen, T.; de Oteyza, D. G., Magnetic Interactions Between Radical Pairs in Chiral Graphene Nanoribbons. Nano Lett. 2022, 22 (1), 164-171.
25. Eimre, K.; Urgel, J. I.; Hayashi, H.; Di Giovannantonio, M.; Ruffieux, P.; Sato, S.; Otomo, S.; Chan, Y. S.; Aratani, N.; Passerone, D.; Gröning, O.; Yamada, H.; Fasel, R.; Pignedoli, C. A., On-surface synthesis and characterization of nitrogen-substituted undecacenes. Nat. Commun. 2022, 13 (1), 511.
26. Biswas, K.; Yang, L.; Ma, J.; Sánchez-Grande, A.; Chen, Q.; Lauwaet, K.; Gallego, J. M.; Miranda, R.; Écija, D.; Jelínek, P.; Feng, X.; Urgel, J. I., Defect-Induced π-Magnetism into Non-Benzenoid Nanographenes. Nanomaterials 2022, 12 (2), 224.
27. Urgel, J. I.; Mishra, S.; Hayashi, H.; Wilhelm, J.; Pignedoli, C. A.; Di Giovannantonio, M.; Widmer, R.; Yamashita, M.; Hieda, N.; Ruffieux, P.; Yamada, H.; Fasel, R., On-surface light-induced generation of higher acenes and elucidation of their open-shell character. Nat. Commun. 2019, 10 (1), 861.
28. Su, J.; Telychko, M.; Hu, P.; Macam, G.; Mutombo, P.; Zhang, H.; Bao, Y.; Cheng, F.; Huang, Z.-Q.; Qiu, Z.; Tan Sherman, J. R.; Lin, H.; Jelínek, P.; Chuang, F.-C.; Wu, J.; Lu, J., Atomically precise bottom-up synthesis of π-extended [5]triangulene. Sci. Adv. 5 (7), eaav7717.
29. Friedrich, N.; Brandimarte, P.; Li, J.; Saito, S.; Yamaguchi, S.; Pozo, I.; Peña, D.; Frederiksen, T.; Garcia-Lekue, A.; Sánchez-Portal, D.; Pascual, J. I., Magnetism of Topological Boundary States Induced by Boron Substitution in Graphene Nanoribbons. Phys. Rev. Lett. 2020, 125 (14), 146801.
30. Mishra, S.; Yao, X.; Chen, Q.; Eimre, K.; Gröning, O.; Ortiz, R.; Di Giovannantonio, M.; Sancho-García, J. C.; Fernández-Rossier, J.; Pignedoli, C. A.; Müllen, K.; Ruffieux, P.; Narita, A.; Fasel, R., Large magnetic exchange coupling in rhombus-shaped nanographenes with zigzag periphery. Nat. Chem. 2021, 13 (6), 581-586.
31. Biswas, K.; Urgel, J. I.; Ajayakumar, M. R.; Ma, J.; Sánchez-Grande, A.; Edalatmanesh, S.; Lauwaet, K.; Mutombo, P.; Gallego, J. M.; Miranda, R.; Jelínek, P.; Feng, X.; Écija, D., Synthesis and Characterization of peri-Heptacene on a Metallic Surface. Angew. Chem. Int. Ed. 2022, n/a (n/a), e202114983.
32. Su, J.; Telychko, M.; Song, S.; Lu, J., Triangulenes: From Precursor Design to On-Surface Synthesis and Characterization. Angew. Chem. Int. Ed. 2020, 59 (20), 7658-7668.
33. Chen, Z.; Narita, A.; Müllen, K., Graphene Nanoribbons: On-Surface Synthesis and Integration into Electronic Devices. Adv. Mater. 2020, 32 (45), 2001893.
34. Houtsma, R. S. K.; de la Rie, J.; Stöhr, M., Atomically precise graphene nanoribbons: interplay of structural and electronic properties. Chem. Soc. Rev. 2021, 50 (11), 6541-6568.
35. Zhou, X.; Yu, G., Modified Engineering of Graphene Nanoribbons Prepared via On-Surface Synthesis. Adv. Mater. 2020, 32 (6), 1905957.
36. Liu, J.; Feng, X., Synthetic Tailoring of Graphene Nanostructures with Zigzag-Edged Topologies: Progress and Perspectives. Angew. Chem. Int. Ed. 2020, 59 (52), 23386-23401.
37. González-Herrero, H.; Gómez-Rodríguez, J. M.; Mallet, P.; Moaied, M.; Palacios, J. J.; Salgado, C.; Ugeda, M. M.; Veuillen, J.-Y.; Yndurain, F.; Brihuega, I., Atomic-scale control of graphene magnetism by using hydrogen atoms. Science 2016, 352 (6284), 437-441.
38. Li, Q.; Lin, H.; Lv, R.; Terrones, M.; Chi, L.; Hofer, W. A.; Pan, M., Locally Induced Spin States on Graphene by Chemical Attachment of Boron Atoms. Nano Lett. 2018, 18 (9), 5482-5487.

39. Ugeda, M. M.; Brihuega, I.; Guinea, F.; Gómez-Rodríguez, J. M., Missing Atom as a Source of Carbon Magnetism. Phys. Rev. Lett. 2010, 104 (9), 096804.
40. Landauer, R., Irreversibility and Heat Generation in the Computing Process. IBM Journal of Research and Development 1961, 5 (3), 183-191.
41. Löwdin, P.-O., Quantum Theory of Many-Particle Systems. I. Physical Interpretations by Means of Density Matrices, Natural Spin-Orbitals, and Convergence Problems in the Method of Configurational Interaction. Phys. Rev. 1955, 97 (6), 1474-1489.
42. Head-Gordon, M., Characterizing unpaired electrons from the one-particle density matrix. Chem. Phys. Lett. 2003, 372 (3), 508-511.
43. Chen, Q.; Thoms, S.; Stöttinger, S.; Schollmeyer, D.; Müllen, K.; Narita, A.; Basché, T., Dibenzo[hi,st]ovalene as Highly Luminescent Nanographene: Efficient Synthesis via Photochemical Cyclodehydroiodination, Optoelectronic Properties, and Single-Molecule Spectroscopy. J. Am. Chem. Soc. 2019, 141 (41), 16439-16449.
44. Gröning, O.; Wang, S.; Yao, X.; Pignedoli, C. A.; Borin Barin, G.; Daniels, C.; Cupo, A.; Meunier, V.; Feng, X.; Narita, A.; Müllen, K.; Ruffieux, P.; Fasel, R., Engineering of robust topological quantum phases in graphene nanoribbons. Nature 2018, 560 (7717), 209-213.
45. Chen, Q.; Schollmeyer, D.; Müllen, K.; Narita, A., Synthesis of Circumpyrene by Alkyne Benzannulation of Brominated Dibenzo[hi,st]ovalene. J. Am. Chem. Soc. 2019, 141 (51), 19994-19999.
46. Hapala, P.; Kichin, G.; Wagner, C.; Tautz, F. S.; Temirov, R.; Jelínek, P., Mechanism of high-resolution STM/AFM imaging with functionalized tips. Phys. Rev. B 2014, 90 (8), 085421.
47. Gross, L.; Mohn, F.; Moll, N.; Liljeroth, P.; Meyer, G., The Chemical Structure of a Molecule Resolved by Atomic Force Microscopy. Science 2009, 325 (5944), 1110.

Insert Table of Contents artwork here